IJNRD.ORG ISSN : 2456-4184
INTERNATIONAL JOURNAL OF NOVEL RESEARCH AND DEVELOPMENT (IJNRD) | IJNRD.ORG
An International Open Access, Peer-reviewed, Refereed Journal

# review paper on black hole

**Abul Hasan**
**Student**
**Lovely Professional University**

## Introduction:

**Stephen Hawking transformed physics between 1974 and 1975 by positing that black holes have temperature, entropy, and gradually evaporate** (Pinochet, 2019)**.**

**When higher-curvature interactions are considered, a mild version of the weak gravity conjecture (WGC) states that extremal black holes have charge-to-mass ratios greater or equal to one. Because these corrections become more relevant in the low-mass regime, the decay of extremal black holes in terms of energy and charge conservation would be possible. Evidence in this direction has mostly come from corrections to Einstein-Maxwell theory. Corrections to the charge-to-mass ratio of some dyonic extremal black holes explicitly embedded in the heterotic string effective theory are computed here. We discover that the extremality bound changes depending on the solution, with the charge-to-mass ratio remaining constant or deviating positively from one. Furthermore, we observe that the inclusion of higher-curvature terms increases the Wald entropy in all cases considered, and that its variation does not appear to be correlated with the charge-to-mass ratio, contrary to Einstein-Maxwell theory** (Cano et al., 2020)**.**

**We investigate the onset of spin-induced scalarization of a black hole in scalar-Gauss-Bonnet gravity with a massive scalar field .Our method is based on the time evolution of the relevant linearized scalar field perturbation equation (2 + 1). We investigate the region where the black hole becomes unstable, resulting in the formation of new scalarized rotating black holes with massive scalar fields. As the scalar field mass increases, so does the minimum value of the Gauss-Bonnet coupling parameter at which scalarization is possible, and thus the instability region shrinks. Surprisingly, the addition of scalar field mass has no effect on the critical minimal value of the black hole angular momentum acrit/ M** (Doneva et al., 2020)**.**

## Properties of Black Holes:

### Black-hole fbinaries' X-ray properties

**We examine the properties and behaviour of 20 X-ray binaries, 17 of which are transient systems, that contain a dynamically confirmed black hole. Using the large-area timing detector aboard the Rossi X-Ray Timing Explorer, many of these transient sources were observed daily over the course of their typically year-long outburst cycles over the last decade. These transient sources' evolution is complicated. Nonetheless, there are behaviour patterns that are shared by all of them, as demonstrated in a comprehensive comparison of six selected systems. Three X-ray states of accretion are reviewed and quantified as the focal point of this comparison. We discuss relativistically broadened Fe lines, high-frequency quasi-periodic oscillations (100-450 Hz), and relativistic radio and X-ray jets that occur in strong gravitational fields. Such phenomena reveal how a black hole interacts with its surroundings, adding to the picture of black holes provided by gravitational wave detectors. We sketch a scenario for the potential impact of accreting black hole timing/spectral studies on physics and discuss a current frontier topic, namely the measurement of black hole spin** (Remillard & McClintock, 2006)**.**

### Identifying the population characteristics of spinning black holes

**At least two formation scenarios are compatible with the first gravitational-wave observations of binary black hole mergers. Black hole binaries are formed in field models from stellar binaries that may undergo common envelope evolution. In dynamic models, black hole binaries are formed by globular cluster capture events. Both types of models have significant theoretical uncertainties. Despite this, conventional wisdom holds that the spin orientation distribution of dynamically merging black holes is nearly isotropic, whereas field-model black holes prefer to spin in alignment with the orbital angular momentum. We present a framework for measuring ensemble properties of black hole spin, such as the typical black hole spin misalignment, using observations of black hole mergers. We show how to obtain population hyperparameter constraints with minimal assumptions, so that the results are not heavily reliant on the uncertain physics of formation models. These data-driven constraints will help theoretical models be tested and the formation history of binary black holes be determined using information encoded in their observed spins. We show how the ensemble**

**properties of binary detections can be used to find and characterise two distinct populations of black hole mergers** (Talbot & Thrane, 2017)**.**

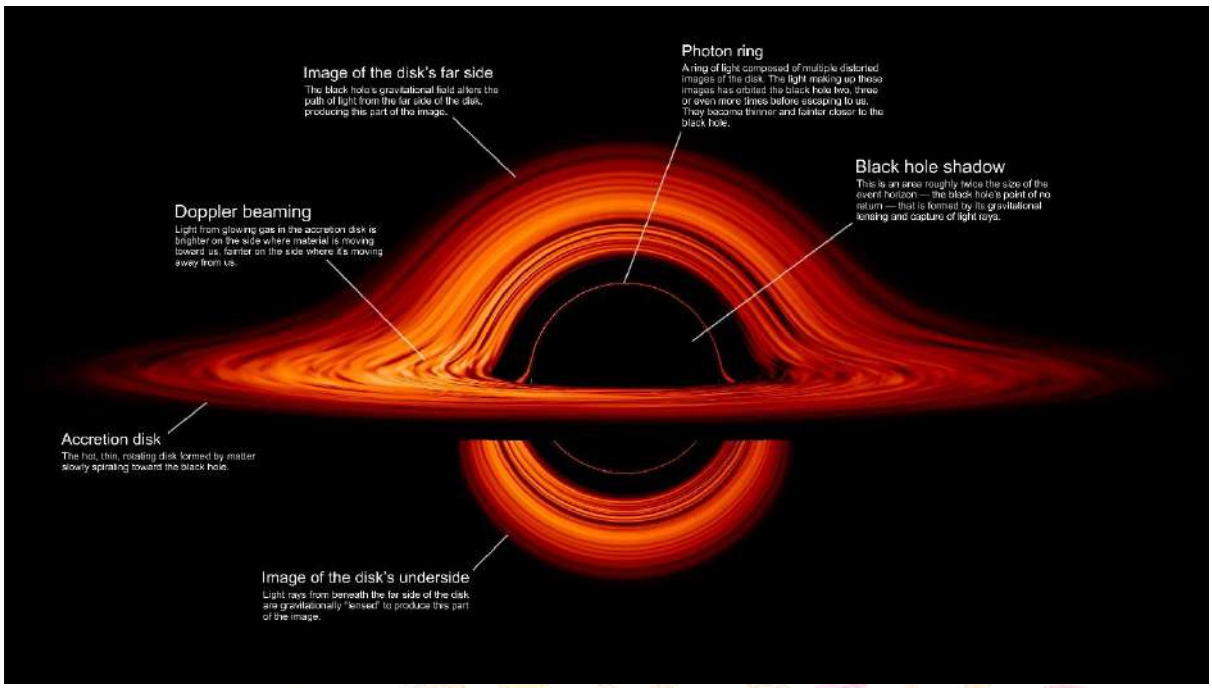


**NASA SVS | Black Hole Accretion Disk Visualization**

## SDSS-IV/SPIDERS: A catalogue of selected X-ray AGN properties SPIDERS SDSS DR14 type 1 AGN spectral properties and black hole mass estimates

**The catalogue of optical spectral properties for all X-ray selected SPIDERS active galactic nuclei (AGN) up to SDSS DR14. SPIDERS (Spectroscopic Identification of EROSITA Sources) is an SDSS-IV programmed that is currently conducting optical spectroscopy of the counterparts to the X-ray selected sources detected in the ROSAT all-sky survey and the XMM-Newton slew survey in the Extended Baryon Oscillation Spectroscopic Survey's footprint . The SPIDERS DR14 sample is the largest X-ray selected AGN sample to date with optical spectroscopic follow-up. The catalogue presented here is based on a clean sample of 7344 2RXS (z = 0:5) and 1157 XMM-Newton slew survey (z = 0:4) type 1 AGN with H and/or MgII emission line spectroscopic coverage. For each object in this sample, visual inspection results are available from a combination of literature sources and the SPIDERS group, which provides both reliable redshifts and source classifications. Using the single-epoch (or photoionisation) method, the spectral regions surrounding the H and MgII emission lines were fitted in order to measure both line and continuum properties, estimate bolometric luminosities, and provide black hole mass estimates. The use of both H and MgII allows for the estimation of black hole masses up to z 2:5. The spectral properties and black hole mass estimates derived from H and MgII are compared using a subsample of objects**

**with coverage of both lines in their spectrum. These findings have been made public as an SDSS-IV DR14 value addition** (Coffey et al., 2019)**.**

**Across cosmic time, the properties of merging black holes and neutron stars**

**The next generation of ground-based gravitational wave interferometers may detect mergers of binary black holes (BBHs) and binary neutron stars (BNSs) with redshifts of z 10 and 2, respectively. We use population-synthesis simulations combined with the ILLUSTRIS cosmological simulation to characterise the properties of merging BBHs, BNSs, and neutron star-black hole binaries across cosmic time. We discover that the mass of merging compact objects is unaffected (or only slightly affected) by the merger redshift. Even the mass distribution of black holes (BHs) is only mildly affected by redshift because BBHs originating from metal-poor progenitors (Z 4 10-3) dominate the entire population of merging BBHs throughout cosmic time. The main difference between the mass distribution of BBHs merging in the last Gyr and that of BBHs merging more than 11 Gyr ago for a common-envelope efficiency 3 is that there is an excess of heavy merging BHs (20-35 M) in the last Gyr. The longer delay time of massive BBHs** (Mapelli et al., 2019)**.**

**Charged Anti-de Sitter Black Hole Microstructures' Repulsive Interactions and Universal Properties**

**The Ruppeiner geometry of thermodynamic fluctuations is a powerful tool for analysing black hole microstructures. We investigate this for charged anti-de Sitter black holes and discover that, while an attractive microstructure interaction dominates for most parameter ranges, a weak repulsive interaction dominates for small high-temperature black holes. This distinguishes the black hole system from a van der Waals fluid, which only has attractive microstructure interactions. We also discover two new universal properties of charged black holes. The repulsive interaction is unaffected by black hole charge or temperature. The other is that the behaviour of the Ruppeiner curvature scalar near criticality is characterised by a dimensionless constant that is identical to that of a van der Waals fluid, revealing new information about black hole microstructures** (Wei et al., 2019)**.**

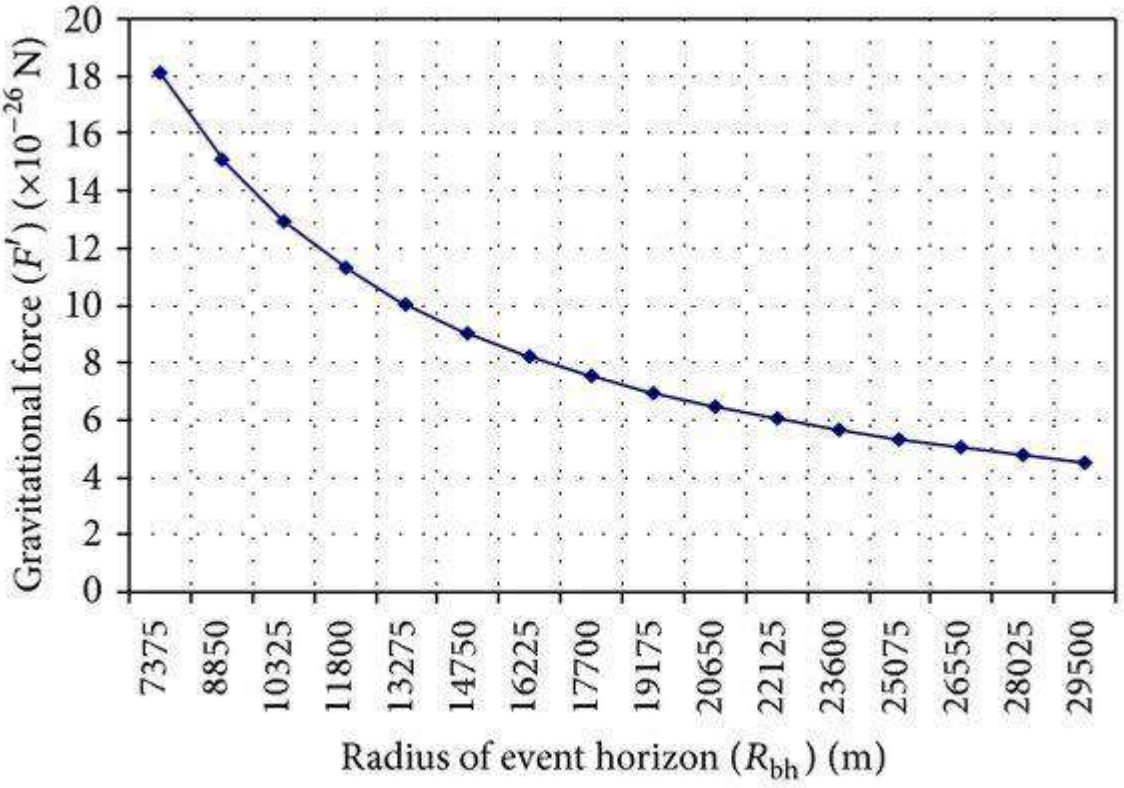


**The graph plotted between the radius of event horizon and Gravitational Force**

## Black hole thermodynamic properties in de Sitter space

**The thermodynamic properties of the Schwarzschild-de Sitter (SdS) and Reissner-Nordström-de Sitter (RNdS) black holes in terms of global and effective thermodynamic quantities. We can calculate the effective thermodynamic quantities of de Sitter black holes using the effective first law of thermodynamics. These effective thermodynamic quantities are discovered to satisfy the Smarr-like formula. In particular, the effective temperatures in the Nariai limit are nonzero. We discover that SdS black holes are always thermodynamically stable, whereas RNdS black holes may undergo phase transitions at some points by calculating heat capacity and Gibbs free energy** (H. F. Li et al., 2017)**.**

International Journal of Novel Research and Development
Research Through Innovation

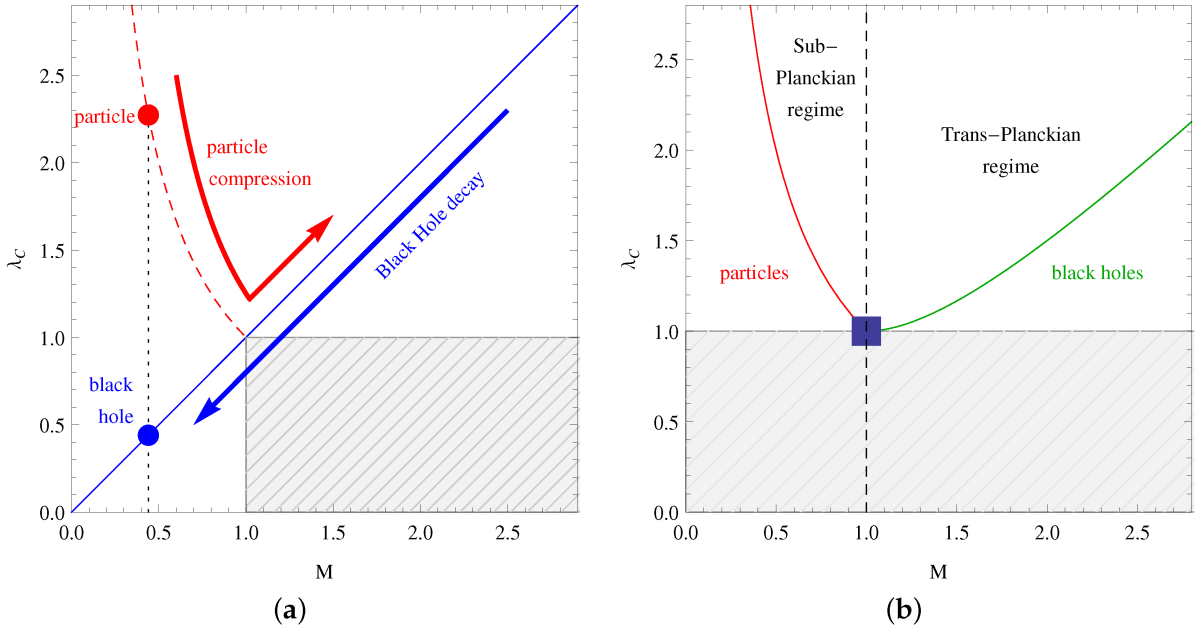


**Entropy | Free Full-Text | Geometric Model of Black Hole ...**

## Absorption effects in the spectral and polarisation properties of black hole accretion disc emission

**The study of radiation emitted by black hole (BH) accretion discs is critical for understanding the main physical properties of these sources, specifically the BH spin. Aside from spectral analysis, polarimetry is becoming increasingly important, driven by the development of new techniques that will soon allow measurements to be performed in X- and -rays. Photons emitted from soft BH accretion discs are expected to be polarised, with an energy dependence that can provide an estimate of the BH spin. However, previous calculations considered scattering to be the only process for determining the polarisation state of the emitted radiation, implicitly assuming that the temperatures involved are such that the material in the disc is completely ionised. We generalise the problem in this work by first calculating the ionisation structure of a surface layer of the disc using the public code cloudy, and then determining the polarisation properties of the emerging radiation using the Monte Carlo code stokes. This allows us to account for absorption effects in addition to scattering effects. We show that incorporating absorption can significantly alter the polarisation properties of the emerging radiation in comparison to what is obtained in the pure-scattering limit. As a general rule, the polarisation degree increases when absorption is greater, as it is for low accretion rates and/or spins when matter ionisation in the innermost accretion disc regions is far from complete** (Taverna et al., 2021)**.**

## OB star-black hole system properties derived from detailed binary evolution models

**Recent gravitational wave measurements have shown that stellar mass black hole binaries exist. The contribution of binary evolution to the formation of double black holes is critical for our understanding of massive star evolution. Aims. Investigating the progenitors of double black hole systems and comparing predictions with local massive star samples, such as the population in 30 Doradus in the Large Magellanic Cloud, is a promising way forward (LMC). Methods. With this goal in mind, we examined a large grid of detailed binary evolution models at LMC metallicity with initial primary masses ranging from 10 to 40? M?, and identified model systems that could potentially evolve into a binary composed of a black hole and a massive main-sequence star. The observable properties of such systems, as well as the peculiarities of the OB star component, were then deduced. Results. When stars with final helium core masses greater than 6.6? M? are assumed to form black holes, we find that 3% of the LMC late-O and early-B stars in binaries are expected to have a black hole companion. While the vast majority of them may be X-ray quiet, our models suggest that they can be identified in spectroscopic binaries by large amplitude radial velocity variations (? 50 km s-1) and simultaneous nitrogen surface enrichment, or by a moderate radial velocity variation (? 10 km s-1) and simultaneous rapid rotation of the OB star. In most cases, the predicted mass ratios allow main-sequence companions to be ruled out. Our conclusion is supported by comparisons to observed OB+WR binaries in the LMC, Be and X-ray binaries, and known massive black hole binaries. We anticipate that spectroscopic observations will be able to test key assumptions in our models, which will have important implications for the evolution of massive stars in general and the formation of double black hole mergers in particular** (Langer et al., 2020).

## The characteristics of discrete black hole hair

**We revisit the physical effects of discrete Z p gauge charge on black hole thermodynamics, building on Coleman, Preskill, and Wilczek's seminal work. We consider the two limiting cases of interest when realising the discrete theory from the spontaneous breaking of an Abelian gauge theory, depending on whether the Compton wavelength of the massive vector is much smaller or much larger than the size of the black hole — the so-called thin- and thick-string limits, respectively. The qualitative effect of discrete hair on the mass-temperature relationship is the same in both regimes and is similar to that of unbroken U(1) charge: a black hole**

**carrying discrete gauge charge is always colder than its uncharged counterpart. In the thick-string limit, our findings call into question some of Coleman et alfindings, .'s as we discuss. Furthermore, we argue that by considering the system to be enclosed within a finite cavity, the unbroken limit can be smoothly defined and the unscreened electric field of the standard Reissner-Nordström solution recovered** (Garcia Garcia, 2019)**.**

**A link between the properties of supermassive black holes, galaxies, and dark matter haloes.**

**In a sample of 55 nearby galaxies with dynamically measured $M rm BHgt 106, rm M odot$ and $M rm hgt 5times 1011, rm M odot$, we investigate the relationships between the mass of the central black hole (BH) MBH, the dark matter halo mass Mh, and the stellar-to-halo mass fraction f?M/Mh. The main difference between this study and previous ones is that we consider both early- and late-type systems, with Mh determined either by globular cluster dynamics or by spatially resolved rotation curves. In the MBH-Mh-f space, galaxies in our sample build a well-defined sequence regardless of their structural properties. We find that: (i) Mh and MBH strongly correlate with each other and anticorrelate with f⋆; (ii) there is a break in the slope of the MBH-Mh relation at Mh of $10^{12}\, {\rm M} \odot$, and in the f⋆-MBH relation at MBH of $\sim 10^7\!-\!10^8\, {\rm M} \odot$; (iii) at a fixed MBH, galaxies with a larger f⋆ tend to occupy lighter haloes and to have later morphological types. We demonstrate that the observed trends can be reproduced by a simple equilibrium model in the CDM framework in which galaxies smoothly accrete dark and baryonic matter at a cosmological rate, with stellar and BH build-up regulated by both the cooling of the available gas reservoir and the negative feedback from star formation and active galactic nuclei (AGNs). Feature (ii) emerges as the BH population transitions from a rapidly accreting to a more gentle and self-regulated growth phase, whereas scatter in AGN feedback efficiency can account for feature I (iii)** (Marasco et al., 2021)**.**

**Using gravitational waves to measure the properties of nearly extreme black holes**

**One of the most important scientific goals for gravitational-wave observations is to characterise the properties of black holes. Astrophysical evidence suggests that black holes with nearly extremal spins (spins close to the theoretical upper limit) may exist and thus be among the merging black holes observed with gravitational waves. We investigate how well current gravitational wave parameter estimation methods can measure the spins of rapidly spinning black holes in binaries in this paper. For nearly-extremal, merging black holes, we simulate gravitational-wave**

**signals using numerical-relativity waveforms. To keep things simple, we'll stick to binaries with spins that are parallel or antiparallel to the orbital angular momentum. We discover that recovering the nearly extremal spins of the holes is difficult. When the spins are nearly extremal and parallel, the resulting parameter estimates recover large spins, though the recovered spin magnitudes are still significantly smaller than the true spin magnitudes. When the spins are nearly extremal and antiparallel to each other, the parameter estimates recover the small effective spin but overestimate the individual spins. We investigate the impact of spin priors and contend that a commonly used prior (uniform in spin magnitude and direction) impedes unbiased recovery of large black-hole spins** (Chatziioannou et al., 2018)**.**

## GW150914 Binary Black Hole Merger Properties

**The Laser Interferometer Gravitational-Wave Observatory (LIGO) detected a gravitational-wave transient (GW150914) on September 14, 2015; we characterise the source's properties and parameters. The data collected around the time of the event was analysed in real time across the LIGO network using a suite of precise waveform models that describe gravitational waves from a compact binary system in general relativity. GW150914 was created by a binary black hole with nearly equal masses of 36-4+5M and 29-4+4M; for each parameter, we report the median value and the range of the 90% credible interval. At 90% probability, the dimensionless spin magnitude of the more massive black hole is bound to be 0.7. According to standard cosmology, the luminosity distance to the source is 410-180+160 Mpc, corresponding to a redshift of 0.09-0.04+0.03. The source is constrained to a 610 deg2 annulus section, primarily in the southern hemisphere. The binary merges to form a black hole with a mass of 62-4+4M and a spin of 0.67-0.07+0.05. This black hole is much more massive than any other black hole inferred from electromagnetic observations in the stellar-mass regime** (Abbott et al., 2016)**.**

## The 150 M Binary Black Hole Merger GW190521 and Its Astrophysical Implications

**When compared to previously reported events, the gravitational-wave signal GW190521 is consistent with a binary black hole merger source at redshift 0.8 with unusually high component masses, $85+21 -14,M odot$ and $66+17 -18,M odot$, and shows mild evidence for spin-induced orbital precession. The primary falls within the mass gap predicted by (pulsational) pair-instability supernova theory, roughly $65 - 120,M odot$. There is a 99.0% chance that at least one of the black holes in GW190521 is in that range. The merger's final mass $(142+28 -16,M odot)$ classifies it as an intermediate-mass black hole. We detail the physical properties**

**of GW190521's source binary and its post-merger remnant, including component masses and spin vectors, under the assumption of a quasi-circular binary black hole coalescence. Three different waveform models, as well as a direct comparison to numerical general relativity solutions, produce consistent estimates of these properties. Strong-field general relativity tests targeting the merger-ringdown stages of coalescence show that the observed signal is consistent with theoretical predictions. The merger rate of similar systems is estimated to be $0.13+0.30 -0.11,rm Gpc-3,rmyr-1$. The astrophysical implications of GW190521 for stellar collapse and the formation of black holes in the pair-instability mass gap via various channels, including (multiple) stellar coalescence and hierarchical merger of lower-mass black holes in star clusters or active galactic nuclei. We believe that GW190521 is a strongly lensed signal from a binary merger of two lower-mass black holes. We also go over some of the more unusual possible sources for GW190521, such as a highly eccentric black hole binary or a primordial black hole binary** (Abbott et al., 2016)**.**

## Types of black holes

1. **Stellar black holes**

   **It is well established that the Inter Galactic Medium (IGM) underwent a "phase transformation" from cold and fully neutral to warm (104 K) and ionised between 380000 and 1 billion years after the Big Bang. The extent to which this phase transformation was driven and completed by photoionization by young hot stars is a topic of current cosmological interest. Aims. We propose that, in addition to ultraviolet radiation from massive stars, feedback from accreting black holes in high-mass X-ray binaries (BH-HMXBs) was a significant source of heating and reionization of the IGM in low-density regions far from star-forming galaxies. Methods. We infer that a significant fraction of the first generations of massive stars end up as BH-HMXBs by using current theoretical models on the formation and evolution of primitive massive stars of low metallicity, as well as observations of compact stellar remnants in the near and distant universe. The total number of energetic ionising photons emitted by an accreting stellar black hole in an HMXB is comparable to that of its progenitor star. The X-ray photons emitted by the accreting black hole, on the other hand, are capable of producing several secondary ionisations, and the resulting black hole's ionising power may be greater than that of its progenitor. Feedback from large populations of BH-HMXBs heats the IGM to 104 K and keeps it ionised over large distance scales. Conclusions. BH-HMXBs determine the early thermal history of the**

**universe and keep it ionised over large areas of space in low density regions. This has a direct impact on the properties of the faintest galaxies at high redshifts, the smallest dwarf galaxies in the local universe, and existing and future surveys of atomic hydrogen in the early universe at radio wavelengths. © 2011 ESO** (Mirabel et al., 2011)**.**

**In globular clusters, stellar black holes**

**Following the discovery of X-ray sources in globular clusters, 1-3 suggested that matter accretion onto a central massive black hole could be a possible explanation. Following that, it was discovered 4,5 that these sources could be easily explained by thermonuclear instabilities on neutron-star surfaces, and black-hole models were abandoned. However, we show here that the recent discovery6 of large populations of millisecond pulsars - and thus neutron stars - in globular clusters implies that hundreds of stellar black holes (of about ten solar masses) should form within a typical cluster. We find that in clusters with a high central density, the rapid dynamical evolution of the black-hole population causes the ejection of nearly all of the holes on a relatively short time scale. However, in intermediate density systems, some of the surviving holes may capture a normal star and form a low-mass X-ray binary. We believe that one or more such binaries may exist in the globular clusters that surround our Galaxy. These systems will be dormant for the most part, with only occasional X-ray outbursts, but future observations of the hard X-ray spectrum may indirectly confirm their existence. Nature Publishing Group, 1993** (Kulkarni et al., 1993)**.**

**Stellar black holes' dynamical evolution in globular clusters**

**According to our current understanding of the stellar initial mass function and massive star evolution, young globular clusters (GCs) could have formed hundreds to thousands of stellar-mass black holes (BHs), the remnants of stars with initial masses ranging from 20 to 100 M. Some BHs may be ejected from their birth clusters by supernova explosions, but the majority should be retained. We investigate the long-term dynamical evolution of GCs containing a large number of stellar BHs using a Monte Carlo method. We present numerical results for 42 models with a wide range of realistic starting conditions, including up to 1.6 106 stars. Almost all models retain a significant number of BHs (up to 103) all the way to the present. This contradicts previous theoretical predictions that most BHs would be dynamically ejected within a few giga years. The main reason for this difference is that core collapse caused by BHs (via the Spitzer "mass segregation instability") is easily reversed by three-body processes, and only**

**a small number of the most massive BHs are involved, whereas lower-mass BHs remain well-mixed with ordinary stars far from the central cusp. As a result, the rapid segregation of stellar BHs does not result in the long-term physical separation of most BHs into a dynamically decoupled inner core, as was previously assumed. When combined with recent detections of several BH X-ray binary candidates in Galactic GCs, our findings suggest that stellar BHs may still be present in large numbers in many GCs today, and that they may play an important role in shaping the long-term dynamical evolution and present-day dynamical structure of many clusters** (Morscher et al., 2015)**.**

**On the most massive stellar black holes**

**The spectrum of compact object masses: neutron stars and black holes (BHs) originating from single stars in various environments is presented. We specifically calculate the maximum BH mass's dependence on metallicity and some specific wind mass loss rates (e.g., Hurley et al. and Vink et al.). Our calculations show that stellar models and the wind mass loss rates used here can explain the highest mass BHs observed in the Galaxy, M bh 15 M, in the high metallicity environment (Z = Z = 0.02). To achieve this result, we used luminous blue variable mass loss rates of 10-4 M yr-1 and metallicity-dependent Wolf-Rayet winds. The maximum BH mass obtained for moderate metallicity (Z = 0.3 Z = 0.006) with such winds, calibrated on Galactic BH mass measurements, is M bh,max = 30 M. This is an interesting discovery because the most massive known stellar BH has a mass of M bh = 23-34 M and is located in a small star-forming galaxy with moderate metallicity. We discover that the maximum BH mass in a very low (globular cluster-like) metallicity environment can be as high as M bh,max = 80 M (Z = 0.01 Z = 0.0002). The X-ray luminosity from Eddington-limited accretion onto an 80 M BH is of the order of 1040 erg s-1, which is comparable to the luminosities of some known ultra-luminous X-ray sources. We emphasise that our findings are for single stars only, and that binary interactions may change these maximum BH masses (e.g., accretion from a close companion). This is purely a proof-of-concept study that shows stellar models can naturally explain even the most massive known stellar BHs. The American Astronomical Society, 2010. All intellectual property rights are reserved** (Belczynski et al., 2010)**.**

**The impact of stellar-mass black holes on Cen's central kinematics: A cautionary tale for IMBH interpretations**

**The observation of a central cusp in the surface brightness profile and a rise towards the centre in the velocity dispersion profiles is frequently used to search for intermediate-mass black holes (IMBHs) in the centres of globular**

**clusters. Similar signatures could, however, result from other effects that must be considered in order to determine the presence (or absence) of an IMBH in these stellar systems. Following on from our previous investigation of the role of radial anisotropy in shaping these observational signatures, we examine the effects produced by the presence of a population of centrally concentrated stellar-mass black holes here. We fit dynamical models to Cen data and show that models with 5% of their mass in black holes can reproduce the data (consistent with 100% retention fraction after natal kicks). When both radial anisotropy and mass segregation are considered simultaneously, the best-fit model has a smaller population of remnants and a less extreme degree of anisotropy than models that only include one of these features. These findings highlight the importance of properly accounting for the effects of stellar-mass black holes and radial anisotropy before drawing conclusions about putative IMBHs** (Kulkarni et al., 1993; Morscher et al., 2015)**.**

**2.**

**Formation of Black Holes:**

**The gravitational collapse of a massive primordial gas cloud is thought to be a promising early universe path for the formation of supermassive blackholes. We investigate the conditions for the formation of so-called direct collapse (DC) blackholes in a fully cosmological context. A semianalytic model of early galaxy formation is combined with halo merger trees built from dark matter $N$-body simulations. We find a total of 68 potential DC sites in a volume of $20;h-1;mathrmMpc$ on a side. We then run hydrodynamic simulations on 42 different halos to study the evolution of the massive clouds within them in great detail. Only two successful cases of gas clouds rapidly collapsing to form stars are found. The tidal force exerted by a nearby massive halo, which would otherwise serve as a radiation source required for DC, prevents gravitational collapse in the other cases. Ram pressure stripping disturbs the approaching cloud. A DC halo and its nearby light source halo frequently merge before the onset of cloud collapse. Only when the DC halo is formed through major mergers does the gas density rise rapidly enough to cause gravitational instability. Based on our cosmological simulations, we conclude that the event rate of DC is an order of magnitude lower than previously reported, though the absolute rate remains unconstrained. To determine the critical radiation flux for DC, the dynamical evolution of a DC cloud and its nearby halo(s) must be followed** (Chon et al., 2016)**.**

## The formation of the first black hole with full numerical relativity

**Using 3+1D numerical relativity simulations, we investigate the formation of black holes from subhorizon and superhorizon perturbations in a matter-dominated universe. We discover that, depending on the initial perturbation's mass and geometry, there are two primary mechanisms of formation: direct collapse of the initial overdensity and post-collapse accretion of the ambient dark matter. For the latter case, the initial perturbation does not need to satisfy the hoop conjecture in order for a black hole to form. In both cases, the formation process lasts approximately a Hubble time, and the initial mass of the black hole is M BH 10-2 H -1 M Pl2. We discover that, at least initially, the PBH experiences rapid mass growth beyond the self-similar limit M BH H -1. We argue that this implies that the majority of the PBH's final mass is accreted from its surroundings after formation. We calculate the probability of primordial black hole formation during the collapse at horizon re-entry of large fluctuations produced during inflation, such as those associated with an ultra-slow-roll period. We show that it interpolates between a Gaussian at low values of the average density contrast and a Cauchy probability distribution at high values. The corresponding abundance of primordial black holes may be several orders of magnitude greater than the Gaussian abundance. The mass function is also shifted towards larger masses.**(Biagetti et al., 2021; De Jong et al., 2022)

## Supermassive black hole formation

**Evidence suggests that massive black holes exist in the majority of nearby galaxies. A number of relationships have also been established between the MBH mass and host galaxy properties such as bulge mass and velocity dispersion. These findings suggest that central MBHs, while much less massive than the host (0.1%), are linked to galactic structure evolution. A single large galaxy today can be traced back to a stage when it was divided into hundreds of smaller components in hierarchical cosmologies. Did MBH seeds form as efficiently in small roto-galaxies, or did their formation have to wait for the formation of larger galaxies with deeper potential wells? I'll go over some of the physical processes that contribute to the evolution of the massive black hole population in this section. I will discuss the processes of black hole formation for'seed' black holes that are likely to form at early cosmic epochs, as well as possible observational tests of these scenarios. Springer-Verlag, Germany, 2010.**(Marasco et al., 2021) **We discuss the current state of knowledge about the early stages of star formation during cosmic dawn. This includes the first generations of metal-free Population III stars that form in the**

**lowest mass dark matter halos where cooling and condensation of gas with primordial composition is possible at very high redshift (z> 20), as well as the first generation of massive black holes that form at such early epochs, known as black hole seeds. The formation of black hole seeds as end states of Population III star collapse or through direct collapse scenarios is discussed. In particular, in light of recent results from stellar evolution models and numerical simulations of the early stages of galaxy formation, special emphasis is placed on the physics of supermassive stars as potential precursors of direct collapse black holes. In addition, we discuss the role of cosmic radiation produced by the early generation of stars and black holes at high redshift in the reionization process.**(Haemmerlé et al., 2020)

**Formation and Populations of Binary Black Hole Mergers**

**We examine the main physical processes that lead to the formation and merger of stellar binary black holes (BBHs). Massive binary stars can evolve in isolation to form BBHs. One of the main sources of uncertainty about this formation channel is the physics of core-collapse supernovae and the process of common envelope. Alternatively, two black holes in a dense star cluster can collide to form a binary. The dynamical formation channel has a number of consequences for the mass, spin, and orbital properties of BBHs. The majority of known Galactic black holes reside in low-mass X-ray binaries. They are rare and fascinating objects, providing unique information on strong gravity, accretion disc physics, and stellar and binary evolution. There is no doubt that our understanding of the formation of black hole low-mass X-ray binaries has significantly advanced in the past decade. However, some key issues are still unresolved. In this paper we briefly summarize the observational clues and theoretical progress on the formation of black hole low-mass X-ray binaries.**(X. D. Li, 2015; Mapelli, 2020)

**Effects of Black Holes on Surrounding Space-time:**

**When the equivalence of the electric charge and mass of individual black holes is assumed, we consider the grand canonical ensemble of static and extremal black holes. We are calculating the effective mass of a test particle and the mean time dilation at the admissible points of space, taking into account the gravitational action of surrounding black holes. We investigate the effect of the statistics that govern extremal black holes on those quantities after specifying them. Statistics' role in this case is to assign a statistical weight to the configurations of a fixed number of black holes. These weights are derived from Bose-Einstein, Fermi-Dirac, classical, and infinite statistics. The aforementioned characteristics are calculated**

**and visualised using mean field approximation, allowing us to draw conclusions based on the visible effect of each statistic.**(Gavrilik & Nazarenko, 2019) **We investigate a fluctuation current passing through a superconducting ring in a space with the Kerr metric. This attempt aims to investigate a conceptual problem, specifically the question of the condensed state in an extreme space-time. The superconducting ring is supposed to be placed in the space surrounding the Kerr black hole (KBH), so that the KBH's rotating axis penetrates the ring's centre. The formulation is based on the linear Landau-Ginzburg free-energy functional. The resulting fluctuation current exhibits several peculiar characteristics that reflect KBH characteristics; that is, the effect of the Kerr metric causes a shift in superconducting transition temperature as well as a scale change in absolute temperature.**(Kuratsuji & Tsuchida, 2019) **We investigate the spectra produced by the Comptonization of soft photons by cold electrons falling radially free onto a black hole. We employ a Monte Carlo method based on a fully relativistic description of Comptonization in Kerr space-time. In agreement with previous research, we discover that Comptonization on the bulk motion of free fall produces power-law spectra with a photon index of 3. In contrast to previous research, we find that these power-law spectra only extend to energies me c2. We show several effects that result in generic cut-offs of such spectra at several tens of keV, regardless of the physical parameters in the model. This inefficiency in producing photons with energies greater than 100 keV rules out bulk motion Comptonization as a primary radiative process in the soft spectral states of black hole binaries. The normalisation of the power law (below the cut-off) with respect to the peak of the surrounding disc's blackbody emission is typically very low, except for models with disc-plasma overlap, in which case the spectra are very soft, 4. 2005 RAS.**(Niedźwiecki & Zdziarski, 2006)**.**

International Journal of Novel Research and Development
IJNRD
Research Through Innovation

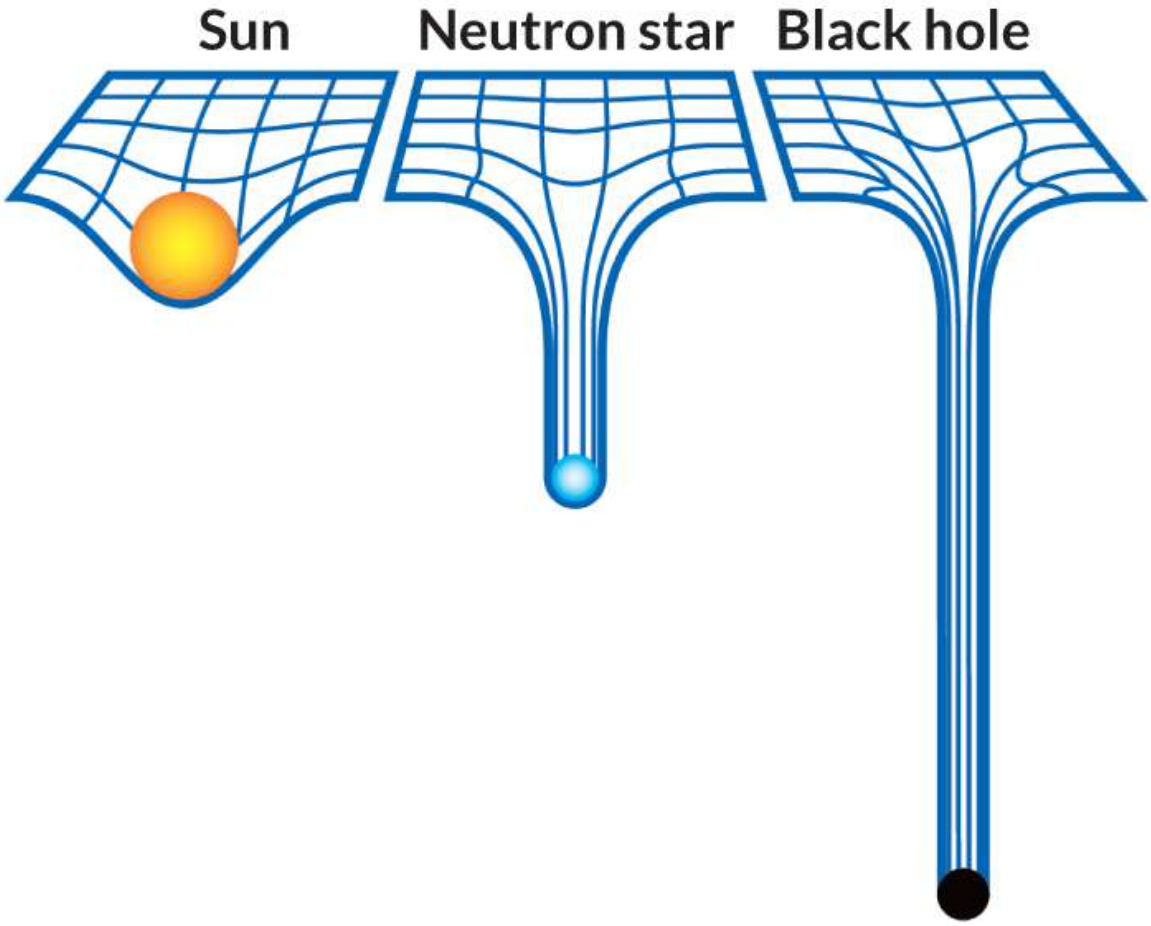


**The mysterious boundary**

**Star-disk interactions in galactic nuclei boost star accretion rates on supermassive black holes.**

**The dynamical interaction of a central star cluster surrounding a supermassive black hole (SMBH) and a central accretion disc is investigated (AD). Because of the rotating AD, the dissipative force acting on stars in the disc causes an enhanced mass flow towards the SMBH and an asymmetry in the phase space distribution. The AD is modelled as a stationary Keplerian rotating disc that has been vertically extended in order to use a fully self-consistent treatment of stellar dynamics that includes the dissipative force resulting from star-gas ram pressure effects. A direct high-accuracy N-body integration code is applied to the stellar system. A star-by-star representation, which is useful in N-body simulations, cannot yet be extended to real particle numbers. As a result, we carefully consider our model's scaling behaviour in terms of particle number and tidal accretion radius. The main idea is to find a family of models in which the ratio of two-body relaxation time to dissipation time (for stellar orbit kinetic energy) is constant, allowing us to extrapolate our results to real parameters of galactic nuclei. Our model is based on fundamental physical principles and thus provides insight into the role of**

**physical processes in galactic nuclei, but it should be viewed as a first step towards more realistic and comprehensive simulations. However, the following conclusions appear to be sound: When compared to purely stellar dynamical systems that ignore the disc, the star accretion rate onto the AD and then onto the SMBH is significantly increased. This process results in increased fueling of central discs in active galactic nuclei (AGNs) as well as an increase in the rate of tidal stellar disruptions. Such disruptions may result in observable X-ray flares as electromagnetic counterparts. In quiescent galactic nuclei, our models improve predictions of their rates. We have not yet modelled direct stellar collisions in the black hole's gravitational potential well, which could increase the black hole's growth rate. Our models are applicable to quiescent galactic nuclei because all of our mass accretion rates result in luminosities much lower than the Eddington luminosity. Other scenarios, such as gas accretion after galaxy mergers, are required to achieve Eddington luminosities, outflows, and feedback as seen in the most active QSOs. Due to the long timescale, this process may not be the dominant accretion process for AGNs close to the Eddington limit. © 2012.**(Just et al., 2012)

**We look at an AGN model with three subsystems:**

**(1) a CSC with mass Mcl describing the galactic center's interior. It is non-rotating, spherically symmetric, and in dynamical equilibrium. (2) An AD with Md = dMcl mass.**

**It has a Keplerian rotation curve and is vertically extended. (3) A central SMBH with Mbh = bhMcl mass.**

**The mutual gravitational interaction of the stars, the gravitational force of the SMBH, and a dissipative force Fd from the AD determine the motion of each star mi of the CSC.**

**The motion equation is given by**

$$\ddot{\boldsymbol{r}}_{\mathrm{i}} = -\sum_{\mathrm{i}\neq\mathrm{j}} \frac{G m_{\mathrm{j}} \boldsymbol{r}_{\mathrm{ij}}}{r_{\mathrm{ij}}^3} - \frac{G M_{\mathrm{bh}} \boldsymbol{r}_{\mathrm{i}}}{r_{\mathrm{i}}^3} + \frac{\boldsymbol{F}_{\mathrm{d}}}{m_{\mathrm{i}}} \quad , \qquad (1)$$

**rij = ri rj, where ri and rj are the positions of stars I and j, respectively. We disregard the gravitating effect of the disc on the system because the AD has a small mass in comparison to the black hole and the enclosed stellar cluster. Section 3 contains numerical details for computing the forces.**

$$\Sigma(R) = \Sigma_{\rm d}\left(\frac{R}{R_{\rm d}}\right)^{-\alpha} \quad \text{with} \quad \alpha = 3/4, \qquad (2)$$

**where R2 = x2 + y2, Rd is the cutoff radius of the disk, and Σd is the surface density at the cutoff radius. The value α = 3/4 corresponds to the outer disk range of NT. The mass Md of the disk is**

$$M_{\rm d} = 2\pi \int_0^{R_{\rm d}} \Sigma(R) R dR = \frac{2\pi}{2-\alpha}\Sigma_{\rm d} R_{\rm d}^2. \qquad (3)$$

**A smooth force in space is required for numerical integration using the fourth-order Hermite scheme. As a result, we implement a continuous but steep outer cutoff by**

$$\Sigma(R) = \Sigma_{\rm d}\left(\frac{R}{R_{\rm d}}\right)^{-\alpha} \exp\left[-\beta_{\rm s}\left(\frac{R}{R_{\rm d}}\right)^{s}\right]. \qquad (4)$$

**The cutoff for s is discontinuous at Rcut = Rd with (1/s) s 1. We'll use s = 4, which gives us s = 0.70 for = 3/4. The surface density at Rd in this case is (Rd) = 0.49 d.**

**An examination of the scaling relations in NT reveals that for SMBHs, self-gravity of the AD for the vertical structure becomes significant for radii greater than 100rS. We simplify the model of the vertical disc structure because we cannot resolve the innermost part of the AD. We use the self-gravitating isothermal profile proposed by**

$$\rho_{\rm g}(R, z) = \frac{\Sigma(R)}{\sqrt{2\pi}h_z} \exp\left(-\frac{z^2}{2h_z^2}\right). \qquad (6)$$

**n the NT model, the (half-)thickness hz increases with distanceaccording ∝ R9/8. Since this is altered by self-gravitation andince we cannot resolve the vertical structure of such a thinisk close to the inner boundary, we decided to adopt a constantthickness hz, taking an appropriate value at some intermediateradius of the AD. To simplify the equations, we define thedimensionless value h = hz/Rd, which is also constant.The effective sound speed cs (which may be dominated bythe turbulent motion in a clumpy gas) is given by (assuming a vertically isothermal model)**

$$c_s^2(R) = 8\pi G\rho_g(R,0)h_z^2 = 4\sqrt{2\pi}G\Sigma h_z$$
$$= \sqrt{\frac{8}{\pi}}(2-\alpha)\frac{\mu_d}{\mu_{bh}}h\left(\frac{R}{R_d}\right)^{1-\alpha} v_{circ}^2(R), \qquad (7)$$

**where vcirc(R) is approximated solely by the SMBH's Kepler rotation. The radial pressure support can be ignored in a thin disc. The rotation curve vcirc is highly supersonic, as shown by Equation (7) (vcirc/cs 100 at the outer boundary Rd for the parameters used in our simulations: bh = 0.1, d = 0.01, and h = 103). The Mach number is decreasing as it moves inward.**

**The sound speed decreases as the radius increases, and the stability of the AD also decreases as the radius increases. The stability parameter Toomre Q is given by**

$$Q^2 = \left(\frac{\kappa c_s}{\pi G\Sigma}\right)^2 = \frac{8}{2-\alpha}\sqrt{\frac{2}{\pi}}\frac{\mu_{bh}}{\mu_d}h\left(\frac{R}{R_d}\right)^{\alpha-3} \qquad (8)$$

**with epicyclic frequency, demonstrating that heavy and thin ADs are unstable near the boundary. For d/bh = 0.1 and h = 103, the AD is formally unstable at R > 0.26Rd. We can ignore this instability in the context of our simplified AD model with constant thickness because it is easily avoided by using an increasing thickness with distance R. The density distribution of the AD with constant thickness (Equation (6)) is given by Equations (2) and (3).**

$$\rho_g(R,z) = \frac{2-\alpha}{2\pi\sqrt{2\pi}}\frac{M_d}{h\,R_d^3}\left(\frac{R}{R_d}\right)^{-\alpha}$$
$$\times \exp\left[-\beta_s\left(\frac{R}{R_d}\right)^s\right]\exp\left(-\frac{z^2}{2h^2R_d^2}\right). \qquad (9)$$

## Stellar Kinetic Energy Dissipation

**A detailed theory of the dissipative force acting on stars crossing the AD is dependent on differential rotation, density profile, turbulent motion in the disc, and potential resonance effects. Stars typically interact with the AD many times supersonically before becoming trapped within it. As a result, we limit our investigation to supersonic motion only, ignoring the details of the final few passages before trapping. In this case, we can use the geometrical cross section Fgeo = Qdr2 gV 2 rel for the dissipative force (determined by the effective area Qdr2 of the bow shock with stellar radius r and Qd 5) enhanced by dynamical friction, which is the gravitational pull by the overdensity in the Mach equation.**

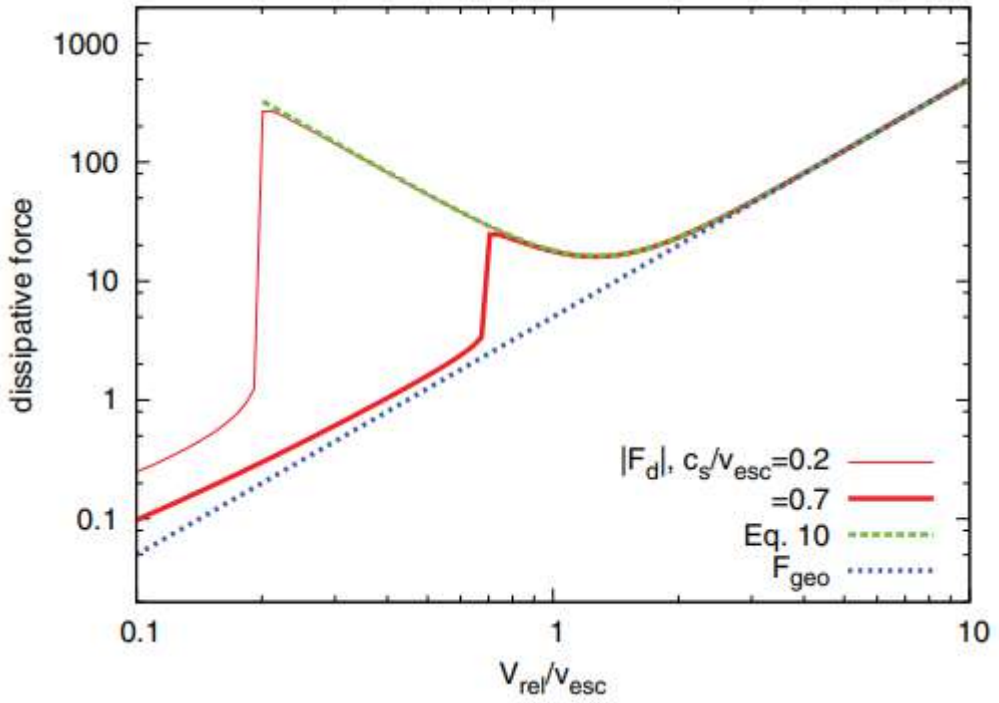


**Figure 1.** Drag force $|F_d|$ in units of $[\pi r_\star^2 \rho_g c_s^2]$ for different sound speeds $c_s$ in the AD (full red lines). We have chosen $Q_d = 5$ and $\ln\Lambda = 13$. The dashed green line shows the approximation given in Equation (10) for the first case. $F_{geo}$ (dotted blue line) is used in the simulations.
(A color version of this figure is available in the online journal.)

$$\boldsymbol{F}_d = -\pi r_\star^2 \rho_g |\boldsymbol{V}_{rel}| \boldsymbol{V}_{rel} \left[ Q_d + \left( \frac{v_{esc}}{V_{rel}} \right)^4 \ln\Lambda \right] \quad \text{for} \quad V_{rel} > c_s. \qquad (10)$$

**The escape velocity at the star's surface is given by vesc (620 km s1 for the Sun) and the relative velocity is given by Vrel = Vd denotes the velocity of the star in the co-rotating frame with the disc.**

**corresponds to the length of the Mach cone in star radius units r, resulting in a Coulomb logarithm ln 10-20.**

**Figure 1 depicts the dissipative force|Fd| for a range of cs/vesc values (full red lines). For cs/vesc = 0.2, the dashed green line represents the approximation given in Equation (10).**

**The dotted blue line depicts Fgeo's contribution to the dissipative force. We expect stars to be quickly decelerated to Vrel cs and onto co-rotating circular orbits, which then move slowly to the centre with a radial decay speed comparable to cs due to the strong dominance of dynamical friction for velocities Vrel smaller than vesc. The dissipative force is anti-parallel to the relative velocity and can accelerate with respect to the CSC's rest frame. To calculate the efficiency of the dissipative force, we first introduce a dissipative timescale tdiss, which describes the energy change**

**E(sd) of a single star due to the dissipative force Fd arising from interaction with the AD at the disk's outer edge. Our strategy is**

$$t_{\mathrm{diss}\star} = \frac{\xi_{\mathrm{k}} m_\star \sigma_\star^2}{P_{\mathrm{d}} \dot{E}_\star^{(\mathrm{sd})}} \qquad (11)$$

**with stellar mass m and three-dimensional stellar velocity dispersion; the dissipative timescale as defined above is strongly influenced by radius. At the AD's outer edge Rd, we have for example E (sd) = Qdr2 g3, g = d/Rd, tdyn = Rd/, and one gets**

$$t_{\mathrm{diss}\star}(R_{\mathrm{d}}) = \frac{\xi_k}{Q_{\mathrm{d}} P_{\mathrm{d}}} \cdot \frac{\Sigma_\star}{\Sigma_{\mathrm{d}}} \cdot t_{\mathrm{dyn}}. \qquad (12)$$

**The surface density of stars is defined as = m/(r2 ) in the second form of the above equation, which provides useful insights. Because the dissipative timescale associated with a single star is a strongly increasing function of radius, the longest dissipation time can be found at the disk's outer edge, in our case at Rd.**

**We will now look at the quantities k and Pd. The former is defined implicitly by 2E:= km2 (Rd) = GmMcl/Rd. The latter, Pd, accounts for the number of disc passages required by a star before its full kinetic energy is dissipated, as well as an average of the stars' orbital parameters, which gives**

$$P_{\mathrm{d}} = \left\langle g(e, i, R_{\mathrm{d}}/p) \frac{t_{\mathrm{dyn}}}{t_{\mathrm{orb}}} \right\rangle. \qquad (13)$$

**In the equation above, the average is taken over all disc crossing events with the proper efficiency function g(e,i,R/p), which depends on the orbital eccentricity e, the inclination with respect to the AD I and the focal parameter p (the properties of g(e,i,R/p) will be discussed in detail in a subsequent paper). For the sake of simplicity, we ignore the contribution of dynamical friction. It is simple to include by replacing Qd in the definition of Pd with the velocity-dependent factor (Qd + (vesc/Vrel) 4 ln).**

$$t_{\mathrm{rx}} = \frac{0.14N}{\ln(0.4N)} t_{\mathrm{dyn}} \quad \text{with} \quad t_{\mathrm{dyn}} = \left( \frac{r_{\mathrm{half}}^3}{G M_{\mathrm{cl}}} \right)^{1/2}, \qquad (14)$$

**where rhalf is the CSC's half-mass radius. Table 1 shows the half-mass relaxation time trx for a series of galactic nuclei spanning the observed range of SMBH masses.**

**The local relaxation time trc caused by two-body interactions is given by**

$$t_{\rm rc} = \frac{0.34\sigma^3}{G^2 m_{\rm s}\rho_{\rm s}\ln\Lambda} = \frac{18{\rm Gyr}}{\ln\Lambda}\left(\frac{\sigma}{1{\rm km\,s^{-1}}}\right)^3\left(\frac{1\,M_\odot}{m_{\rm s}}\right)\left(\frac{1\,M_\odot{\rm pc^{-3}}}{\rho_{\rm s}}\right) \quad (15)$$

**with one-dimensional velocity dispersion, mean particle mass ms, and CSC density s. This equation, which is also known as the core relaxation time, can be applied at each radius or to the central region of a system by using mean values inside some radius r. We assume 2 r1 inside the black hole's gravitational influence radius rh (which is of the same order as the disk's outer radius Rd in our model), and the standard Bahcall-Wolf (BW) density cusp solution for the stellar density profile in the CSC is r7/4. As a result, we get trc r1/4 for the local relaxation time.**

**Table 1**
Some Examples for the Physical Scaling of Galactic Nuclei

| Object | $M_{\rm bh}$ ($M_\odot$) | $\sigma_{\rm c}$ (km s$^{-1}$) | $r_{\rm h}$ (pc) | $N$ | $t_{\rm dyn}$ (Myr) | $t_{\rm rx}$ (Gyr) | $Q_{\rm tot}$ | $Q_{\rm tot}(8k)$ | $L_{\rm max}$ ($L_\odot$) |
|---|---|---|---|---|---|---|---|---|---|
| M 87 | $6.6\times10^9$ | 312 | 291 | $6.6\times10^{10}$ | 1.5 | $6\times10^5$ | $2.1\times10^{-9}$ | $5.7\times10^{-3}$ | $1\times10^8$ |
| NGC 3115 | $9.6\times10^8$ | 230 | 78 | $9.6\times10^9$ | 0.58 | $3.4\times10^4$ | $4.2\times10^{-9}$ | $1.8\times10^{-3}$ | $2.8\times10^7$ |
| NGC 4291 | $3.2\times10^8$ | 242 | 24 | $3.2\times10^9$ | 0.16 | 3400 | $1.5\times10^{-8}$ | $2.4\times10^{-3}$ | $9.4\times10^7$ |
| M 31 | $1.5\times10^8$ | 160 | 25 | $1.5\times10^9$ | 0.26 | 2690 | $6.2\times10^{-9}$ | $4.7\times10^{-4}$ | $5\times10^7$ |
| NGC 4486A | $1.3\times10^7$ | 111 | 4.5 | $1.3\times10^8$ | 0.067 | 68.8 | $1.7\times10^{-8}$ | $1.2\times10^{-4}$ | $1.9\times10^8$ |
| MW | $4\times10^6$ | 110 | 1.4 | $4\times10^7$ | 0.021 | 7.2 | $5.2\times10^{-8}$ | $1.2\times10^{-4}$ | $5\times10^8$ |
| M 32 | $3\times10^6$ | 75 | 2.3 | $3\times10^7$ | 0.050 | 12.9 | $1.5\times10^{-8}$ | $2.8\times10^{-5}$ | $2\times10^8$ |

**Notes.** For the CSC, we adopt $\mu_{\rm bh} = 0.1$, solar-type stars with $m_\star = 1\,M_\odot$, $r_\star = 2.3\times10^{-8}$ pc, $v_{\rm esc} = 620$ km s$^{-1}$, $R_{\rm d} = r_{\rm h}$ and $r_{\rm half} = 3r_{\rm h}$, and $Q_{\rm d} = 5$ for the bow shock size. Most observational data (Columns 2 and 3) are taken from Gültekin et al. (2009), improved values for M 87 are from Murphy et al. (2011), and $M_{\rm bh}$ for the Milky Way (MW) is from Gillessen et al. (2009). The influence radius (Column 4) is derived from $r_h = GM_{\rm bh}/\sigma_c^2$, with the core velocity dispersion $\sigma_c$ of the CSC; $N$ is the number of stars in the CSC derived from $M_{\rm bh}/\mu_{\rm bh}$; the dynamical and half-mass relaxation timescales (Columns 6 and 7) are derived by Equation (14); the physical and scaled cross sections $Q_{\rm tot}$ and $Q_{\rm tot}(8k)$ (Columns 8 and 9) by Equations (19) and (21); and the maximum luminosity by accretion (Column 10) assuming $L_{\rm max} = 0.1\dot{M}_{\rm bh}c^2$.

**The influence radius trc(rh) is 1.5-2 times shorter than trx. This demonstrates that our confined model with a CSC accurately represents two-body relaxation in the central part of galactic nuclei.**

**Only ten times the mass of the SMBH.**

**It is more practical to define a global dissipation timescale tdiss and a global dimensionless dissipative timescale in the following way for comparison with measurements in our simulations, as described later.**

$$\eta = t_{\rm diss}/t_{\rm rx} \quad (16)$$

$$t_{\rm diss} = \frac{E_k}{\dot{E}^{(sd)}} = \frac{M_{\rm cl}\sigma_\star^2(r_{\rm acc})}{2\dot{E}^{(sd)}} = \frac{GM_{\rm bh}M_{\rm cl}}{2r_{\rm acc}\dot{E}^{(sd)}}.$$

**Ek is the total kinetic energy and total energy dissipation rate of all stars at the accretion radius, with 2Ek = Mcl2 (racc) = GMclMbh/racc and E (sd). The accretion time scale for black hole growth is defined by tacc = Mbh/M bh, or v = tacc/trx in dimensionless form. In a stationary state, the energy dissipation rate required at racc to sustain the black hole mass accretion rate is E(sd) = M bhGMbh/ (2racc).**

**Equation (16) yields**

$$\nu = \frac{t_{\rm acc}}{t_{\rm rx}} = \eta \frac{t_{\rm acc}}{t_{\rm diss}} = \eta \quad \frac{M_{\rm bh}}{\dot{M}_{\rm bh}} \quad \frac{\dot{E}^{\rm (sd)}}{E_k} = \eta \mu_{\rm bh}. \qquad (17)$$

## THE MATHEMATICAL MODEL

**We used the specially developed GRAPE (= Parallel Hermite Integration with GRAPE) code for the high resolution direct N-body simulations of the CSC. The programme employs the fourth-order Hermite integration scheme for particles with hierarchical individual block time steps, as well as the parallel use of GRAPE6 (or nowadays the GPU: Graphics Processing Unit) cards for the hardware calculation of the acceleration a and its first time derivative a In this section, we will briefly discuss the most important features added to the Hermite scheme of the N-body GRAPE code to model the ram pressure dissipative force and star accretion to the SMBH.**

**1. A dissipative force routine in which we calculate the acceleration ad (Equation (20)) and its first time derivative a d caused by the interaction with the gaseous disc.**

**2. When stars approach the disc plane, we reduce their time steps. Otherwise, stars with a large individual time step may miss the disc and not feel its effect at all.**

**3. A simple stellar accretion scheme onto the SMBH, in which stellar mass is added to the central black hole if it falls within a certain accretion radius. The accretion radius is used as a free scaling parameter; results for different accretion radii can be scaled to real galactic nuclei parameters (see Section 4.2). Fiestas et al. (2011) and Li et al. (2011) described and used this algorithm (2012).**

**4. To control integration error, we add careful bookkeeping of energy changes caused by removing stars during the accretion process as well as the dissipative force of the stars-gas interaction. The total energy error in any of our runs does not exceed 104.**

$$G = M_{\rm cl} = 4|E_{\rm tot}| = 1, \qquad (18)$$

**An analytic Kepler potential fixed at the origin is used to model the SMBH with initial mass Mbh = bhMcl. We allow accretion of stars, which are effectively captured by the inner part of the AD or scattered into the loss cone by two-body relaxation, to increase the mass of the SMBH. Physically, the accretion radiusracc is given by the tidal radius rt, or the Schwarzschild radius rS, where the stars are disrupted. Both radii are several orders of magnitude smaller than our numerical resolution. As a result, we must investigate the scaling of the accretion with decreasing accretion radius.**

**Before being accreted, the orbits of the stars accreted by the interaction with the AD are circularised. Stars accreted into the loss cone by two-body scattering, on the other hand, are predominantly. . In order to simulate the effect**

**of the different eccentricity distribution, we apply a second**

**accretion criterion based on the velocity of the stars. We define**

**an accretion criterion to merge stars with the SMBH using two**

**criteria: (1) distance r<racc and (2) V 2**

**< kaccv2**

**circ. Stars well**

**inside the influence radius of the SMBH are moving on (local)**

**Kepler orbits, where the velocity is given by V 2**

**= v2**

**circ(2−r/a)**

**with semimajor axis a. In the limit of large kacc, all stars reaching**

**racc would be accreted. For kacc = 1, stars inside racc are**

**accreted if a racc, i.e., all stars with energy below −GMcl/racc**

**(neglecting the potential energy of the CSC) are accreted in one**

**orbital time. In all simulations, we use kacc = 1. (Note for**

**completeness that in some runs with AD we accreted all stars**

**with r<racc/10 independent of their energy. We have tested**

**that the accretion rates are not changed significantly by this additional accretion criterion.)**

**The properties of the AD are fixed by the normalized mass μd with analytic density distribution according to Equation (6) with α = 3/4, s = 4, and constant thickness h = 10−3. We use a Kepler rotation of the AD in the potential of the SMBH, neglecting the gravity of the CSC and pressure gradients in the AD. We set the outer cutoff initially at Rd = rh. Using a Kepler rotation curve underestimates the real circular speed at the outer boundary by a factor of 1.4, but this has no significant influence on the dynamics of the stars. The reason is that the gas density and thus the friction force is very small in the outer regions of the AD. The part of the AD with significant dissipation of energy of crossing stars is deep inside the influence radius of the SMBH. Here, the approximation of Kepler rotation is very good. We have chosen the large cutoff radius only in order to avoid another free parameter**

$$Q_{\rm tot} = Q_{\rm d} \frac{N \pi r_\star^2}{\pi R_{\rm d}^2}. \qquad (19)$$

**It is worth noting that Qtot multiplies Qd by a factor that describes the dimensionless total dissipative cross section of N stars normalised to disc area. We can rewrite using this definition.**

**the original dissipative force as acceleration in Equation (10)**

$$\boldsymbol{a}_{\rm d} = \boldsymbol{F}_{\rm d}/m_\star = -Q_{\rm tot} \frac{\pi R_{\rm d}^2 \rho_{\rm g}}{M_{\rm cl}} |\boldsymbol{V}_{\rm rel}| \boldsymbol{V}_{\rm rel}. \qquad (20)$$

$$Q_{\rm tot}(N_2) = \frac{t_{\rm rx}(N_1)}{t_{\rm rx}(N_2)} Q_{\rm tot}(N_1). \qquad (21)$$

**In our initial configuration, we added the central SMBH to the CSC's Plummer distribution. To begin the analysis of the system in dynamical equilibrium, we let the CSC evolve with the SMBH for 5tdyn. Following the initialization phase, the cusp around the SMBH has a density slope of 2.5, which differs from a BW cusp (top panel of Figure 2). The difference between the set-up Plummer profile and the cumulative mass profile at t = 0 shows the effect of virialization on the SMBH's potential. Then we calculate Rd so that the enclosed CSC mass at R = Rd equals the SMBH mass at t = 0. We ran a series of simulations with various particle numbers N = 4k, 8k, 16k and accretion radii racc = 0.04, 0.02, 0.01, 0.005 (see Table 2) until t = 10trx. The simulation identifiers in Table 2 encode the particle number and accretion radius. A run without dissipative force is performed for each parameter combination for comparison. We used Equation to scale the scaling for different N. (21).**

International Research Journal
IJNRD
Research Through Innovation

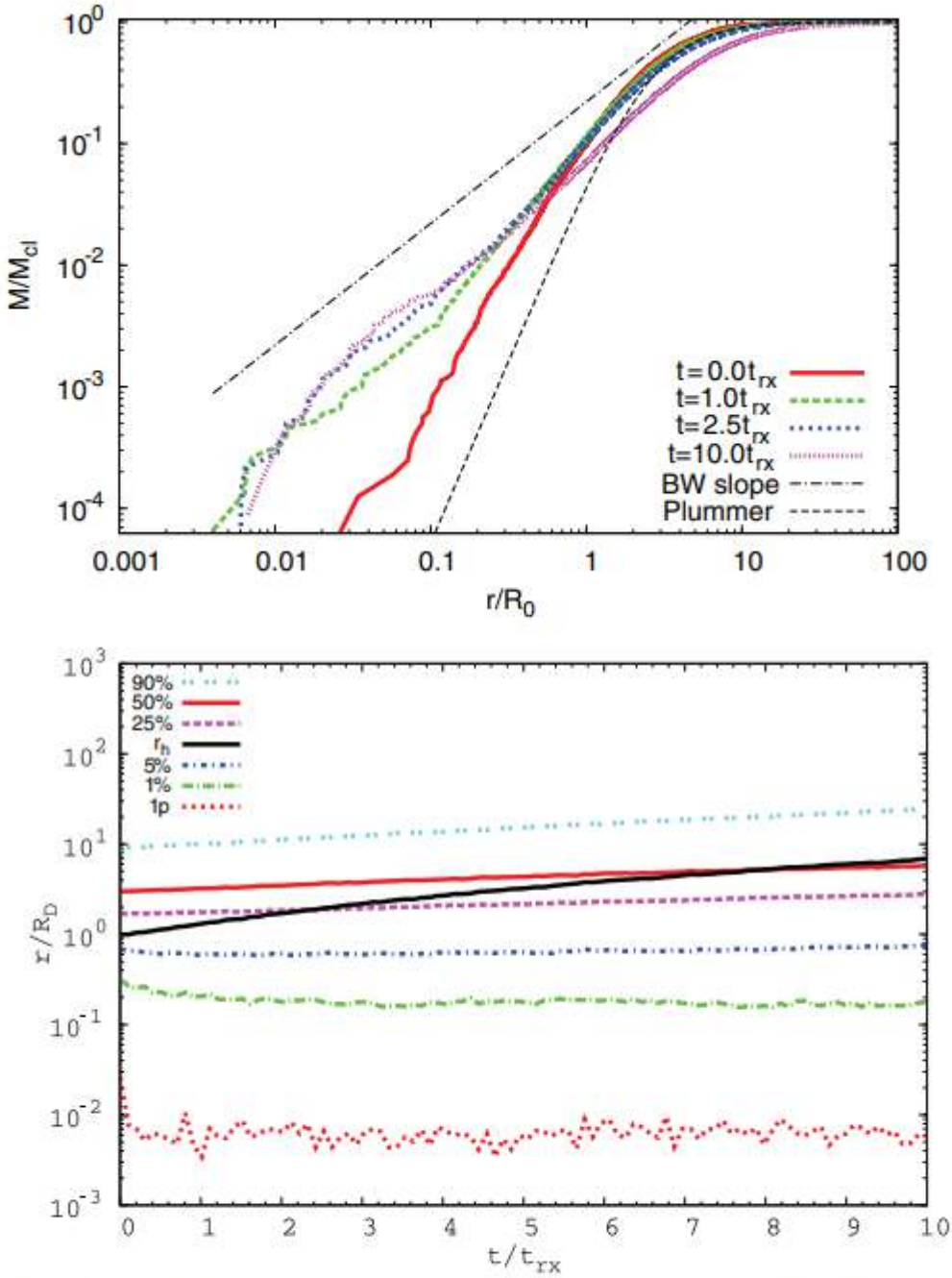


**Figure 2.** Evolution of the CSC for model 16K-005. Top panel: cumulative mass profiles in units of the initial CSC mass at different times with the Plummer profile and the power law of a Bahcall–Wolf (BW) cusp added for comparison. Bottom panel: Lagrange radii enclosing a fixed mass fraction with respect to $M_{cl}(t)$. The position of the innermost particle (1p) and the influence radius $r_h$ are also shown.

**Our choice of Qtot corresponds to the case of M 87 in simulations with dissipative force (compare Tables 1 and 2).**

**The last column in Table 1 shows that the value of Qtot in our simulations for lower mass black holes is unrealistically large.**

**We used parallel GRAPE systems built at the Astronomisches Rechen-Institut in Heidelberg7 and the Fesenkov Astrophysical Institute in Almaty to calculate the CSC dynamics. The code was recently ported to large clusters with GPU hardware (in Beijing, China and Heidelberg, Germany, see acknowledgements), and the**

**results from these facilities were used in part for this project. the CSC is in dynamical equilibrium, including the gravitational potential of the SMBH, and the density profile has a steep cusp. The aggregate**

**The mass profiles in the top panel of Figure 2 show that the BW cusp is in place after one relaxation time and remains stable throughout the simulation. Figure 2's lower panel depicts the Lagrange radii of the CSC for 1%, 5%, 25%, 50%, and 90% enclosed mass in relation to total mass Mcl (t)**

**Table 2**
Model Parameters of All Runs

| Model | $N$ | $\epsilon/R_{\rm d}$ | $r_{\rm acc}/R_{\rm d}$ | $Q_{\rm tot}(N)$ |
|---|---|---|---|---|
| 04K-005 | $4k$ | $4.55\times10^{-4}$ | $5\times10^{-3}$ | $10^{-2}$ |
| 04K-01 | $4k$ | $4.55\times10^{-4}$ | $10^{-2}$ | $10^{-2}$ |
| 04K-02 | $4k$ | $4.55\times10^{-4}$ | $2\times10^{-2}$ | $10^{-2}$ |
| 04K-04 | $4k$ | $4.55\times10^{-4}$ | $4\times10^{-2}$ | $10^{-2}$ |
| 08K-005 | $8k$ | $4.55\times10^{-4}$ | $5\times10^{-3}$ | $5.47\times10^{-3}$ |
| 08K-01 | $8k$ | $4.55\times10^{-4}$ | $10^{-2}$ | $5.47\times10^{-3}$ |
| 08K-02 | $8k$ | $4.55\times10^{-4}$ | $2\times10^{-2}$ | $5.47\times10^{-3}$ |
| 08K-04 | $8k$ | $4.55\times10^{-4}$ | $4\times10^{-2}$ | $5.47\times10^{-3}$ |
| 16K-005 | $16k$ | $4.55\times10^{-4}$ | $5\times10^{-3}$ | $2.97\times10^{-3}$ |
| 16K-01 | $16k$ | $4.55\times10^{-4}$ | $10^{-2}$ | $2.97\times10^{-3}$ |
| 16K-02 | $16k$ | $4.55\times10^{-4}$ | $2\times10^{-2}$ | $2.97\times10^{-3}$ |
| 16K-04 | $16k$ | $4.55\times10^{-4}$ | $4\times10^{-2}$ | $2.97\times10^{-3}$ |

**Notes.** Column 1 gives the identification label of the model, Columns 2–4 are number of particles, smoothing length, and accretion radius. Column 5 gives the total cross section, $Q_{\rm tot}$, scaled according to Equation (21). Common parameters for all models are $\mu_{\rm bh}=0.1$, $\mu_{\rm d}=0.01$, $h=10^{-3}$, and $k_{\rm acc}=1$.

**for the 16K-005 model (see Table 2 for model parameters).**

**Furthermore, the position of the innermost particle (1p) indicates that stars crossing racc on highly eccentric orbits are rapidly circularised and accreted. Because of accretion, the SMBH's influence radius rh grows by an order of magnitude during the simulation, as does the size of the BW cusp.**

## The Radius of Accretion

**The numerical resolution is much larger than the physical accretion radius racc. As a result, the scaling of the accretion rate with racc is critical. With decreasing racc, the loss cone becomes thinner, resulting in a decreasing accretion rate in the limit of an empty loss cone (e.g., Amaro-Seoane & Spurzem 2001). The BW cusp, on the other hand, is distinguished by a constant mass and energy flow to the SMBH, as**

**well as a high binding energy. As a result, the accretion rate determined by an energy criterion should be independent of racc. Figure 5 depicts the independence of the accretion rate on racc in terms of the accretion timescale v (Equation (17)) for all N = 16k runs with dissipative force. The accretion rate is also independent of the particle number N for t > 1 trx.**

**With the parameters chosen for the AD and the CSC, the SMBH's growth timescale by star accretion is of the order of the CSC's half-mass relaxation time trx, which is long compared to the Eddington accretion timescale of 50 Myr (see Table 1). As a result, our model applies to dormant galactic nuclei. By using Lmax = 0.1M bhc2, the accretion rate can be converted to a maximum luminosity. This upper limit applies to all SMBH masses between 2... 50 107 L (last column of Table 1).**

International Research Journal
IJNRD
Research Through Innovation

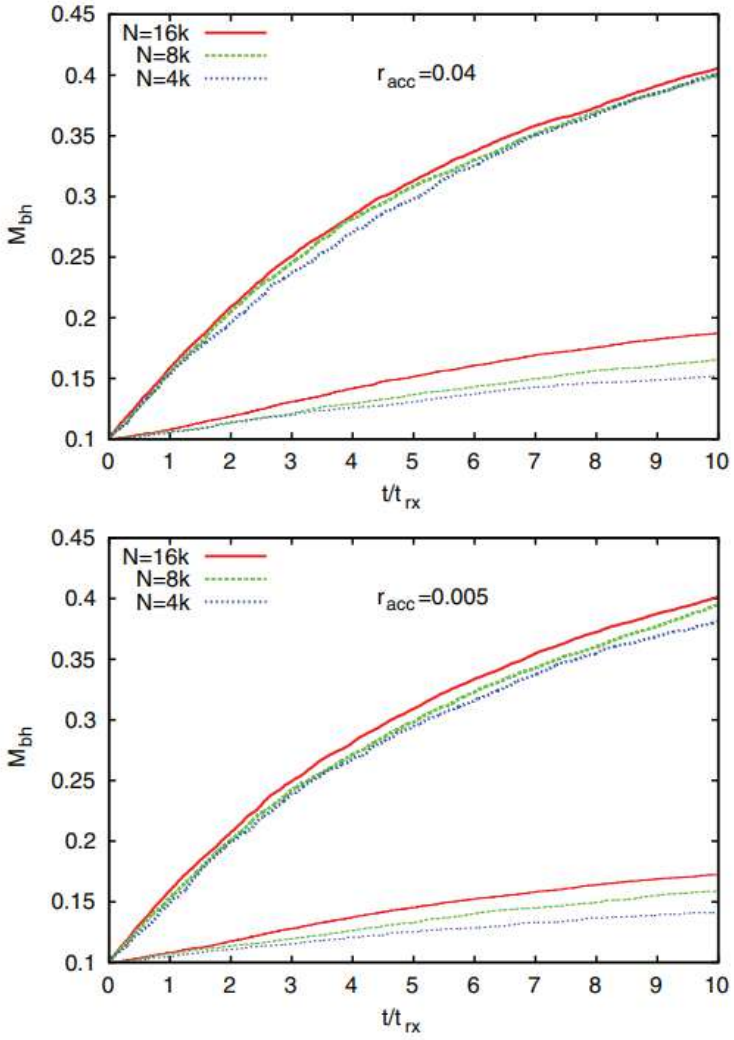


**Figure 3.** SMBH growth with (upper thick lines) and without (lower thin lines) dissipative force for different accretion radii $r_{acc} = 0.04$ (top panel) and $r_{acc} = 0.005$ (bottom panel). The particle number ranges from $N = 4k...16k$. $Q_{tot}$ scales according to Equation (21) with $N$.

(A color version of this figure is available in the online journal.)

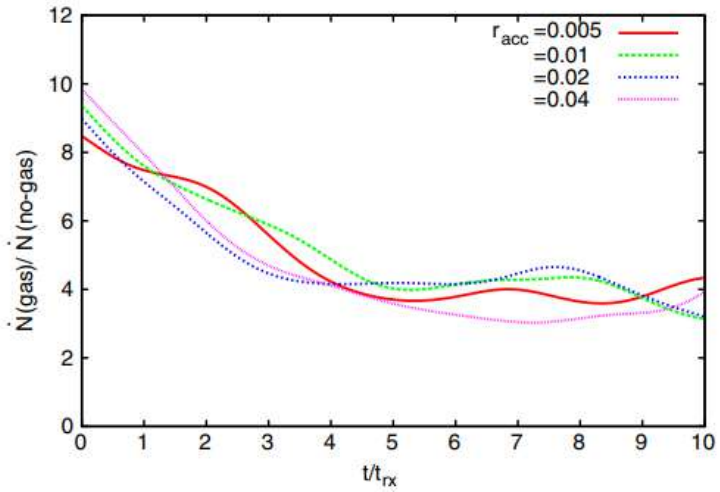


**Figure 4.** Ratio of the accretion rates with and without dissipative force for $N = 8$k and different $r_{acc}$.

(A color version of this figure is available in the online journal.)

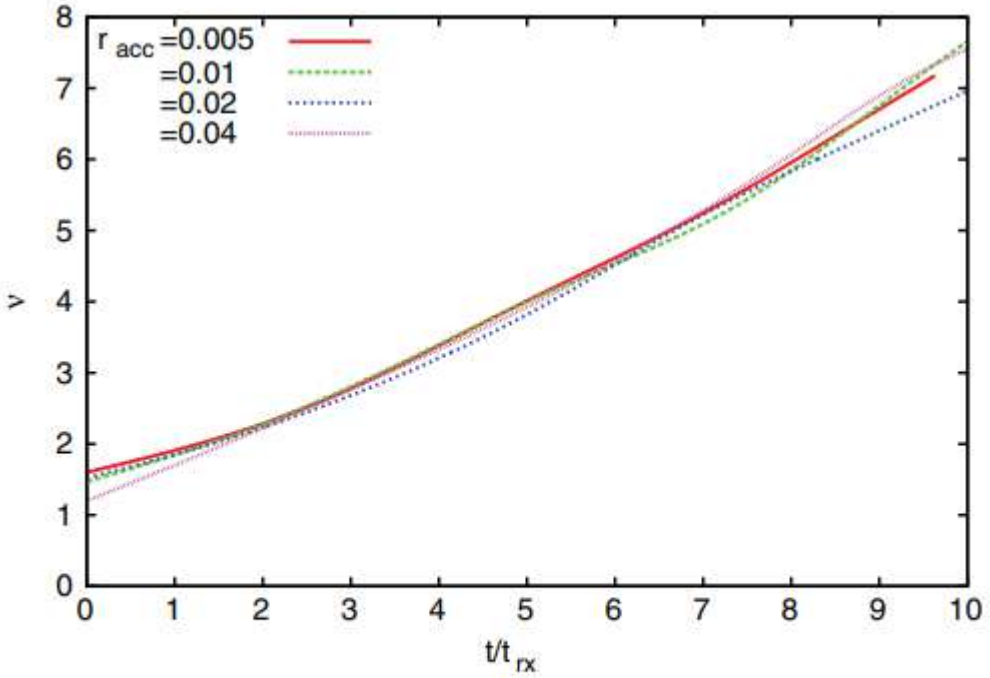


**Figure 5.** Normalized accretion timescale $\nu$ (Equation (17)) for $N = 16k$ with different $r_{acc}$ (same line styles as in Figure 4).
(A color version of this figure is available in the online journal.)

---

**As a result, the accretion rate determined by an energy criterion should be independent of racc. Figure 5 depicts the independence of the accretion rate on racc in terms of the accretion timescale v (Equation (17)) for all N = 16k runs with dissipative force. The accretion rate is also independent of the particle number N for t > 1 trx.**

**With the parameters chosen for the AD and the CSC, the SMBH's growth timescale by star accretion is of the order of the CSC's half-mass relaxation time trx, which is long compared to the Eddington accretion timescale of 50 Myr (see Table 1). As a result, our model applies to dormant galactic nuclei. By using Lmax = 0.1M bhc2, the accretion rate can be converted to a maximum luminosity. This upper limit applies to all SMBH masses between 2... 50 107 L (last column of Table 1).**

## Conclusion:

**Because of its incredible density, the black hole bends spacetime to the point where there is no more space or time. There is a uniqueness. As our experiment demonstrates, the larger the star, the more spacetime curves itself. But we don't know much about black holes, and much of what we do know is theoretical. Only three of their properties are known: their mass, electric charge, and cinetic moment ( if they are in rotation or not). We also know that a black hole's entropy is infinite. The entropy is a measure of the number of possible microscopic element**

**configurations. Because the surface of the black hole expands over time, global entropy increases. This extremely high entropy would result from the transition of a complex object, the original object (such as a star), to an object so'simple' that it is defined by only three factors. There are numerous theories floating around the world about the inside of this unknown celest body. There are also theories about spacetime reversing on the other side of the black hole. That would imply that spacetime curves in the opposite direction.**

**To summarise, black holes are a perplexing topic that has only been proven to exist since 1967 but has been theorised for centuries. They are an aspect of space about which scientists know very little but hope to learn more someday. Black holes are made up of nothing more than a tiny centre piece of mass known as the singularity, which is so compact that not even light can escape. Once an entity has passed a black hole's event horizon, it is doomed (unless it can travel faster than the speed of light... which is impossible). Black holes are fascinating and mysterious. Their characteristics are also somewhat intriguing. Despite the fact that these amazing "space creatures" are invisible, scientists continue to investigate them. Would you like to be one of these scientists who studies black holes? Or would you consider venturing into space and risking your life to get a closer look at black holes? There are many conclusions to everything, but a black hole may never have one. In general, black holes can live for a googol years before dying in a 'evaporation explosion' the size of billions of nuclear bombs. They die as a result of Hawking radiation, which gradually removes mass from the singularity. Although extremely perplexing, black holes are a fascinating topic to investigate and will leave you with many questions that even the brightest scientists do not know the answers to.**

International Journal of Novel Research and Development
IJNRD
Research Through Innovation

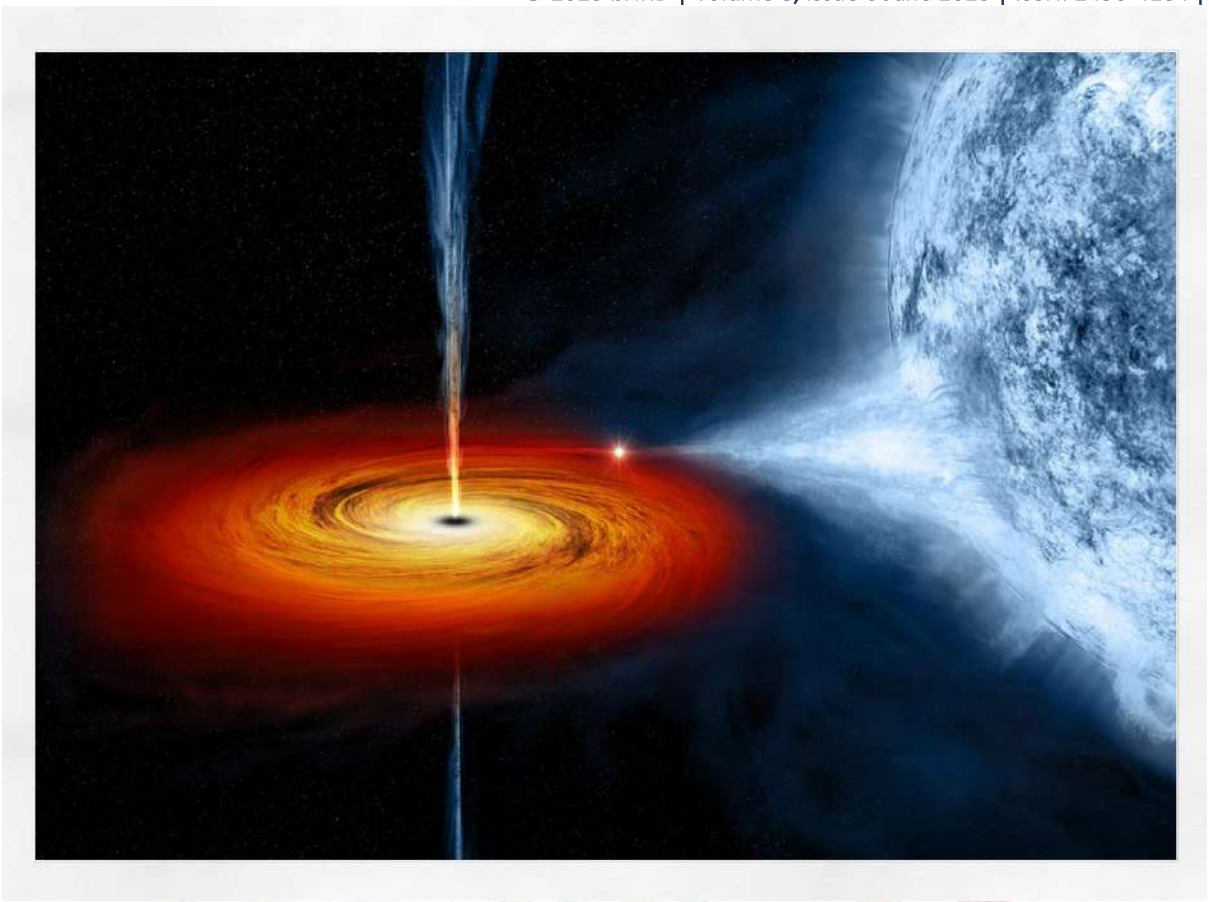

## REFERENCES


Abbott, B. P., Abbott, R., Abbott, T. D., Abernathy, M. R., Acernese, F., Ackley, K., Adams, C., Adams, T., Addesso, P., Adhikari, R. X., Adya, V. B., Affeldt, C., Agathos, M., Agatsuma, K., Aggarwal, N., Aguiar, O. D., Aiello, L., Ain, A., Ajith, P., … Zlochower, Y. (2016). Properties of the Binary Black Hole Merger GW150914. *Physical Review Letters*, *116*(24). https://doi.org/10.1103/PhysRevLett.116.241102

Belczynski, K., Bulik, T., Fryer, C. L., Ruiter, A., Valsecchi, F., Vink, J. S., & Hurley, J. R. (2010). On the maximum mass of stellar black holes. *Astrophysical Journal*, *714*(2). https://doi.org/10.1088/0004-637X/714/2/1217

Biagetti, M., De Luca, V., Franciolini, G., Kehagias, A., & Riotto, A. (2021). The formation probability of primordial black holes. *Physics Letters, Section B: Nuclear, Elementary Particle and High-Energy Physics*, *820*. https://doi.org/10.1016/j.physletb.2021.136602

Cano, P. A., Ortín, T., & Ramírez, P. F. (2020). On the extremality bound of stringy black holes. *Journal of High Energy Physics*, *2020*(2). https://doi.org/10.1007/JHEP02(2020)175

Chatziioannou, K., Lovelace, G., Boyle, M., Giesler, M., Hemberger, D. A., Katebi, R., Kidder, L. E., Pfeiffer, H. P., Scheel, M. A., & Szilágyi, B. (2018). Measuring the properties of nearly extremal black holes with gravitational waves. *Physical Review D*, *98*(4). https://doi.org/10.1103/PhysRevD.98.044028

Chon, S., Hirano, S., Hosokawa, T., & Yoshida, N. (2016). COSMOLOGICAL SIMULATIONS OF EARLY BLACK HOLE FORMATION: HALO MERGERS, TIDAL DISRUPTION, AND THE CONDITIONS FOR DIRECT COLLAPSE. *The Astrophysical Journal*, *832*(2). https://doi.org/10.3847/0004-637x/832/2/134

Coffey, D., Salvato, M., Merloni, A., Boller, T., Nandra, K., Dwelly, T., Comparat, J., Schulze, A., Del Moro, A., & Schneider, D. P. (2019). SDSS-IV/SPIDERS: A catalogue of X-ray selected AGN properties Spectral properties and black hole mass estimates for SPIDERS SDSS DR14 type 1 AGN. *Astronomy and Astrophysics*, *625*. https://doi.org/10.1051/0004-6361/201833996

De Jong, E., Aurrekoetxea, J. C., & Lim, E. A. (2022). Primordial black hole formation with full numerical relativity. *Journal of Cosmology and Astroparticle Physics*, *2022*(3). https://doi.org/10.1088/1475-7516/2022/03/029

Doneva, D. D., Collodel, L. G., Krüger, C. J., & Yazadjiev, S. S. (2020). Spin-induced scalarization of Kerr black holes with a massive scalar field. *European Physical Journal C*, *80*(12). https://doi.org/10.1140/epjc/s10052-020-08765-3

Garcia Garcia, I. (2019). Properties of discrete black hole hair. *Journal of High Energy Physics*, *2019*(2). https://doi.org/10.1007/JHEP02(2019)117

Gavrilik, A. M., & Nazarenko, A. V. (2019). Statistics effects in extremal black holes ensemble. *International Journal of Modern Physics A*, *34*(32). https://doi.org/10.1142/S0217751X19502154

Haemmerlé, L., Mayer, L., Klessen, R. S., Hosokawa, T., Madau, P., & Bromm, V. (2020). Formation of the First Stars and Black Holes. In *Space Science Reviews* (Vol. 216, Issue 4). https://doi.org/10.1007/s11214-020-00673-y

Just, A., Yurin, D., Makukov, M., Berczik, P., Omarov, C., Spurzem, R., & Vilkoviskij, E. Y. (2012). Enhanced accretion rates of stars on supermassive black holes by star-disk interactions in galactic nuclei. *Astrophysical Journal*, *758*(1). https://doi.org/10.1088/0004-637X/758/1/51

Kulkarni, S. R., Hut, P., & McMillan, S. J. (1993). Stellar black holes in globular clusters. *Nature*, *364*(6436). https://doi.org/10.1038/364421a0

Kuratsuji, H., & Tsuchida, S. (2019). Superconducting fluctuation current in a space with the Kerr metric. *EPL*, *126*(1). https://doi.org/10.1209/0295-5075/126/10004

Langer, N., Schürmann, C., Stoll, K., Marchant, P., Lennon, D. J., Mahy, L., De Mink, S. E., Quast, M., Riedel, W., Sana, H., Schneider, P., Schootemeijer, A., Wang, C., Almeida, L. A., Bestenlehner, J. M., Bodensteiner, J., Castro, N., Clark, S., Crowther, P. A., … Xu, X. T. (2020). Properties of OB star-black hole systems derived from detailed binary evolution models. *Astronomy and Astrophysics*, *638*. https://doi.org/10.1051/0004-6361/201937375

Li, H. F., Ma, M. Sen, & Ma, Y. Q. (2017). Thermodynamic properties of black holes in de Sitter space. *Modern Physics Letters A*, *32*(2). https://doi.org/10.1142/S0217732317500171

Li, X. D. (2015). Formation of black hole low-mass X-ray binaries. In *New Astronomy Reviews* (Vols. 64–66). https://doi.org/10.1016/j.newar.2015.02.001

Mapelli, M. (2020). Binary Black Hole Mergers: Formation and Populations. In *Frontiers in Astronomy and Space Sciences* (Vol. 7). https://doi.org/10.3389/fspas.2020.00038

Mapelli, M., Giacobbo, N., Santoliquido, F., & Artale, M. C. (2019). The properties of merging black holes and neutron stars across cosmic time. *Monthly Notices of the Royal Astronomical Society*, *487*(1). https://doi.org/10.1093/mnras/stz1150

Marasco, A., Cresci, G., Posti, L., Fraternali, F., Mannucci, F., Marconi, A., Belfiore, F., & Fall, S. M.

(2021). A universal relation between the properties of supermassive black holes, galaxies, and dark matter haloes. *Monthly Notices of the Royal Astronomical Society*, *507*(3). https://doi.org/10.1093/mnras/stab2317

Mirabel, I. F., Dijkstra, M., Laurent, P., Loeb, A., & Pritchard, J. R. (2011). Stellar black holes at the dawn of the universe. *Astronomy and Astrophysics*, *528*. https://doi.org/10.1051/0004-6361/201016357

Morscher, M., Pattabiraman, B., Rodriguez, C., Rasio, F. A., & Umbreit, S. (2015). The dynamical evolution of stellar black holes in globular clusters. *Astrophysical Journal Letters*, *800*(1). https://doi.org/10.1088/0004-637X/800/1/9

Niedźwiecki, A., & Zdziarski, A. A. (2006). Bulk motion Comptonization in black hole accretion flows. *Monthly Notices of the Royal Astronomical Society*, *365*(2). https://doi.org/10.1111/j.1365-2966.2005.09752.x

Pinochet, J. (2019). "Black holes ain't so black": An introduction to the great discoveries of Stephen Hawking. *Physics Education*, *54*(3). https://doi.org/10.1088/1361-6552/ab0e9a

Remillard, R. A., & McClintock, J. E. (2006). X-ray properties of black-hole fbinaries. *Annual Review of Astronomy and Astrophysics*, *44*. https://doi.org/10.1146/annurev.astro.44.051905.092532

Talbot, C., & Thrane, E. (2017). Determining the population properties of spinning black holes. *Physical Review D*, *96*(2). https://doi.org/10.1103/PhysRevD.96.023012

Taverna, R., Marra, L., Bianchi, S., Dovčiak, M., Goosmann, R., Marin, F., Matt, G., & Zhang, W. (2021). Spectral and polarization properties of black hole accretion disc emission: Including absorption effects. *Monthly Notices of the Royal Astronomical Society*, *501*(3). https://doi.org/10.1093/mnras/staa3859

Wei, S. W., Liu, Y. X., & Mann, R. B. (2019). Repulsive Interactions and Universal Properties of Charged Anti-de Sitter Black Hole Microstructures. *Physical Review Letters*, *123*(7). https://doi.org/10.1103/PhysRevLett.123.071103

https://svs.gsfc.nasa.gov/13326

IJNRD
Research Through Innovation